Energy spectrum of two-dimensional isotropic rapidly rotating turbulence

Pei-Yang Li and Jin-Han Xie*
Department of Mechanics and Engineering Science at College of Engineering, and State Key Laboratory for Turbulence and Complex Systems, Peking University, Beijing 100871, People's Republic of China

(Received 12 November 2024; accepted 28 April 2025; published 19 May 2025)

We study a two-dimensional isotropic rotating system and obtain both theoretically and numerically a K^{-2} energy spectrum under the rapidly rotating condition (Ro $\ll 1$), which was initially obtained by Zeman [Phys. Fluids **6**, 3221 (1994)] and Zhou [Phys. Fluids **7**, 2092 (1995)]. In rotating turbulence, the K^{-2} energy spectrum was proposed under the assumption of isotropy; however, the direction selectivity of rotation breaks isotropy, making this K^{-2} spectrum not easily observable. To fill the gap between theoretical assumptions and realizability, we study the turbulence of inertial waves in an artificial two-dimensional isotropic rotating turbulence system. In the limit of a small Rossby number, we asymptotically derive a nonlinear amplitude equation for inertial waves, which gives the K^{-2} spectrum using a strong turbulence argument. This scaling is justified by numerical simulations of both the amplitude equation and the original system.

DOI: 10.1103/PhysRevFluids.10.054608

I. INTRODUCTION

Rotating turbulence, which is usually considered to be a three-dimensional (3D) anisotropic case, arises in a variety of geophysical and engineering applications, such as atmospheric dynamics, ocean currents, and turbine flows [1–4]. The effect of rotation, as predicted by the Taylor-Proudman theorem, leads to two-dimensional (2D) behavior [5–7], and thus to interesting energy cascade scenarios. With regard to classical homogeneous isotropic turbulence without rotation, energy cascades forward to small scales in the 3D case following the Kolmogorov spectrum $E(K) \sim K^{-5/3}$, with K the wave number, while in the 2D case energy transfer upscales with $E(K) \sim K^{-5/3}$ and enstrophy cascades to small scales with $E(K) \sim K^{-3}$ [8]. 3D rotating turbulence could manifest a dual cascade scenario if the space is infinite and the dissipation scale is small enough, where a forward energy cascade occurs at small scales dominated by eddy viscosity, and an inverse energy cascade appears at large scales dominated by rotation [9–12]. The dual cascade is an important phenomenon in geophysical fluid dynamics, as it helps explain the behavior of atmospheric and oceanic flows, especially the formation of large-scale coherent structures induced by an inverse cascade [13–19].

Without considering anisotropy, Zeman [20] proposed a dual spectrum in rotating turbulence separated by a Zeman wave number $K_Z = (\Omega^3/\epsilon)^{1/2}$, where Ω is the angular velocity and ϵ is the energy dissipation rate. When $K \gg K_Z$, the energy spectrum follows Kolmogorov's theory with scaling $K^{-5/3}$, while when $K \ll K_Z$, the energy spectrum follows $E(K) \sim K^{-2}$. From the perspective of timescale, Zhou [21] argued that the timescale for inducing turbulent spectral transfer is captured by the eddy turnover without rotation, while when rotation is dominant, it is described by the rotating timescale $1/\Omega$, leading to an $E(K) \sim K^{-2}$ spectrum.

*Contact author: jinhanxie@pku.edu.cn

In atmospheric and oceanic flows, where strong rotation is accompanied by stratification, the horizontal spectrum also manifests a $K_\perp^{-2}$ scaling, where the subindex $\perp$ denotes the direction perpendicular to the rotation axis. In the submesoscale $(1 - 20\,\mathrm{km})$ range of the upper-ocean, Callies and Ferrari [22] observed that kinetic-energy spectra showed a $K_\perp^{-2}$ scaling. Then Bühler *et al.* [23] separated the contribution of inertia-gravity waves (IGWs) from that of geostrophic motion and showed that the IGWs part follows a $K_\perp^{-2}$ spectrum in the ocean. They also found a $K_\perp^{-2}$ horizontal kinetic energy spectrum at wavelengths of $1 - 10\,\mathrm{km}$ in the troposphere [24]. In the background of rapidly rotating, strongly stratified turbulence, Kafiabad *et al.* [25] obtained a $K_\perp^{-2}$ spectrum of inertia-gravity waves in a Boussinesq system under the assumption of horizontal isotropy. Although this spectrum is not of the turbulent flow, it may provide additional explanations for the appearance of the observed $K_\perp^{-2}$ spectrum. Savva *et al.* [26] derived a linear kinetic equation to describe the scattering of IGWs by geostrophic turbulence to explain the $K_\perp^{-2}$ spectrum with a cascade from the scale of the internal wave forcing to smaller scales.

The K^{-2} spectrum of rotating turbulence was also obtained by dimensional analysis of wave turbulence theory [27] with a 3D wave resonant triad under the assumption that $k_\parallel \sim k_\perp$, where the subindex $\parallel$ denotes the direction parallel to the rotation axis. However, without the assumption of isotropy, Galtier [28] applied weak wave turbulence theory for 3D incompressible fluids under rapid rotation and analytically found an anisotropic energy spectrum $E \sim k_\perp^{-5/2} k_\parallel^{-1/2}$ when the transfer time given by the wave kinetic equation is much larger than the inertial-wave period. This condition is not valid in the entire wave-number space, and the weak wave turbulence theory does not describe the dynamics of 2D modes at the lowest order, which decouples from 3D waves.

In this paper, we attempt to study whether the isotropic arguments of Zeman [20] and Zhou [21] capture certain key features of rotating turbulence, which is hard due to the naturally introduced anisotropic effect of rotation. Moreover, their discussions are limited by choosing a single finite timescale $1/\Omega$, while in a rotating fluid system, the linear dispersion relation [27]

$$\omega = \pm \sqrt{\frac{(2\Omega)^2 k_\parallel^2}{k_\parallel^2 + k_\perp^2}}, \tag{1}$$

where the frequency of the inertial wave, ω, ranges between 0 and 2Ω, and leads to a wide range of timescale.

To realize the isotropy assumptions by Zeman and Zhou, we introduce an isotropic rotating turbulence system, where the linear inertial waves have only a single timescale. Our idea is to introduce an auxiliary buoyancy effect that resembles the effect of rotation. For example, Rayleigh-Bénard convection, where buoyancy is the primary driver, and Taylor-Couette flow, where rotation is the dominant factor, have a similar ultimate scaling of heat or angular momentum transport [29–31]. Their turbulent statistics and flow structures are also similar when their transport coefficients are chosen to be consistent [32]. Zhang and Sun [33] also showed the similarity between rotation and stratification on wall turbulence, where the Coriolis and buoyancy forces are "twin forces" whose effects can be unified. Thus we can construct an isotropic rotating system by employing appropriate stratification in conjunction with rotation. This system can also avoid the existence of a wide range of timescale.

The structure of the rest of the paper is as follows. In Sec. II, we introduce an idealized isotropic rotating system that perfectly satisfies Zeman's and Zhou's assumptions. By asymptotic expansion, we obtain the equation for the evolution of wave amplitude in Sec. III. In Sec. III C, we predict the existence of the K^{-2} spectrum from the amplitude equation by dimensional analysis under the assumption of strong turbulence. In Sec. IV, numerical simulations of the amplitude equation and original equations both show the K^{-2} spectrum. The differences between the current isotropic system and the classic anisotropic system are also studied. We summarize and discuss our results in Sec. V. We show the consistent spectra of high-order terms in Appendix A, and we discuss the K^{-2} spectrum by using the wave turbulence theory in Appendix B.

II. GOVERNING EQUATIONS

We consider an idealized isotropic rotating stratified system proposed by Xie and Bühler [34], which stems from the inviscid two-dimensional ($\partial_y = 0$) rotating stratified Boussinesq equations [2]

$$u_t + uu_x + wu_z - fv = -p_x, \tag{2a}$$

$$v_t + uv_x + wv_z + fu = 0, \tag{2b}$$

$$w_t + uw_x + ww_z - b = -p_z, \tag{2c}$$

$$b_t + ub_x + wb_z + N^2 w = 0, \tag{2d}$$

$$u_x + w_z = 0, \tag{2e}$$

where u, v, and w are the velocities in the (x, y, z) directions, $f = 2\Omega$ is the Coriolis frequency, b is the buoyancy, and N is the buoyancy frequency. Defining $\theta = b/N$ and introducing a streamfunction ψ such that $(u, w) = \nabla^\perp \psi$ with $\nabla^\perp = (-\partial_z, \partial_x)$, Eqs. (2) in a special *isotropic* case with $f = N$ can be simplified to

$$\nabla^2 \psi_t + \mathcal{J}(\psi, \nabla^2 \psi) - f\theta_x + fv_z = 0, \tag{3a}$$

$$v_t + \mathcal{J}(\psi, v) - f\psi_z = 0, \tag{3b}$$

$$\theta_t + \mathcal{J}(\psi, \theta) + f\psi_x = 0, \tag{3c}$$

where $\mathcal{J}(a, b) = a_x b_z - a_z b_x$.

Introducing the rescaling

$$t \sim 1/f, x \sim L,\ z \sim L,\ v \sim U,\ \theta \sim U,\ \psi \sim UL, \tag{4a}$$

(3) is nondimensionalized to

$$\nabla^2 \psi_t + \mathrm{Ro}\mathcal{J}(\psi, \nabla^2 \psi) - \theta_x + v_z = 0, \tag{5a}$$

$$v_t + \mathrm{Ro}\mathcal{J}(\psi, v) - \psi_z = 0, \tag{5b}$$

$$\theta_t + \mathrm{Ro}\mathcal{J}(\psi, \theta) + \psi_x = 0, \tag{5c}$$

where $\mathrm{Ro} = U/fL$ is the Rossby number, capturing the relative strength between the advection and Coriolis effects. Notably, Eqs. (5b) and (5c) are similar, which shows the similarity between rotation and stratification, and v enters Eq. (5a) similarly to θ, therefore we refer to v and θ as buoyancy scalars and define $\mathcal{E}_p = \int (|v|^2 + |\theta|^2)/2\ \mathrm{d}x\mathrm{d}z$ as the potential energy. Then the kinetic energy is defined as $\mathcal{E}_k = \int |\nabla \psi|^2/2\ \mathrm{d}x\mathrm{d}z$. System (5) preserves a total energy

$$\mathcal{E}_{\mathrm{tot}} = \mathcal{E}_k + \mathcal{E}_p = \int \frac{1}{2}(|\nabla \psi|^2 + |v|^2 + |\theta|^2)\mathrm{d}x\mathrm{d}z. \tag{6}$$

To justify the isotropy of the system (5), we consider a rotation transformation

$$x' = x\cos\alpha - z\sin\alpha, \tag{7a}$$

$$z' = x\sin\alpha + z\cos\alpha. \tag{7b}$$

Letting

$$\psi'(x', z') = \psi(x, z), \tag{8}$$

and defining new scalars as

$$v' = v\cos\alpha - \theta\sin\alpha \quad \text{and} \quad \theta' = v\sin\alpha + \theta\cos\alpha, \tag{9}$$

the system (5) is invariant.

Rotating stratified fluid consists of vortical and wave motions, and we consider their linear decomposition based on the dispersion relation. Considering a small perturbation to a zero state, we obtain linear equations

$$\nabla^2\psi_t' - \theta_x' + v_z' = 0, \tag{10a}$$

$$v_t' - \psi_z' = 0, \tag{10b}$$

$$\theta_t' + \psi_x' = 0, \tag{10c}$$

where the characters with a prime denote perturbation variables. Considering a normal mode, i.e., $\psi' = \tilde{\psi}' e^{-\mathrm{i}\omega t + \mathrm{i}(kx+mz)}$, where k and m are the horizontal and vertical wave numbers, respectively, we obtain the dispersion relation

$$\omega_* = 0 \quad \text{and} \quad \omega_\pm = \pm 1, \tag{11}$$

and the corresponding eigenvectors

$$\begin{bmatrix} \psi_* \\ v_* \\ \theta_* \end{bmatrix} = \begin{bmatrix} 0 \\ k \\ m \end{bmatrix} \quad \text{and} \quad \begin{bmatrix} \psi_\pm \\ v_\pm \\ \theta_\pm \end{bmatrix} = \begin{bmatrix} 1 \\ \pm m \\ \mp k \end{bmatrix}. \tag{12}$$

Here, $_*$ and $_\pm$ denote the vortical and wave components, respectively. It is interesting to note that ψ is only related to the wave part, which we use in Sec. IV B to avoid exciting vortical models in numerical simulations.

This isotropic system (5) with a wave-number-independent dispersion relation perfectly satisfies Zeman's and Zhou's assumptions and choices of a single timescale for the rotation effect. In addition, the nondimensionalized frequency takes two definite values $\omega = \pm 1$, corresponding to Coriolis frequency, therefore triad interaction of a linear wave is not permitted. In comparison, the current isotropic scenario is much simpler than the anisotropic case with $f \neq N$, where the linear dispersion relation for inertia–gravity waves is [2]

$$\omega = \pm\sqrt{\frac{N^2k^2 + f^2m^2}{k^2 + m^2}}, \tag{13}$$

which is anisotropic and could permit a triad wave interaction [27].

III. AMPLITUDE EQUATION

Like the derivation of Young and Ben Jelloul [35] equations for the slow modulation of the amplitude of waves about their rapid oscillation at fast frequency f_0, we derive the slow evolution equation of the wave amplitude by asymptotic expansion under Ro $\ll 1$ to elucidate the nonlinear interaction of weak linear waves and to obtain the corresponding energy spectra of our system (5) under the rapid rotation condition.

A. Reformulating the system (5)

We first introduce a Helmholtz decomposition to the buoyancy scalars

$$(v, \theta) = \nabla\Phi + \nabla^\perp\Psi. \tag{14}$$

Therefore, the polarization relation (12) leads to the constraints on the linear vortical flow ($\omega_* = 0$)

$$\psi = 0, \quad \nabla^2\Psi = 0, \tag{15}$$

and on the linear wave ($\omega_\pm = \pm 1$)

$$\nabla^2\Phi = 0. \tag{16}$$

Thus, considering a suitable boundary condition, e.g., a doubly periodic boundary condition, at the linear level, ψ and Ψ capture the wave component, and Φ describes the vortical flow.

Rewriting Eqs. (5) in terms of ψ, Ψ, and Φ, we obtain

$$\nabla^2\psi_t - \nabla^2\Psi + \mathrm{Ro}\mathcal{J}(\psi, \nabla^2\psi) = 0, \tag{17a}$$

$$\nabla^2\Psi_t + \nabla^2\psi + \mathrm{Ro}(\mathcal{J}(\psi, \nabla^2\Psi) + \mathcal{J}(\psi_x, \Psi_x) + \mathcal{J}(\psi_z, \Psi_z) + \mathcal{J}(\psi_x, \Phi_z) - \mathcal{J}(\psi_z, \Phi_x)) = 0, \tag{17b}$$

$$\nabla^2\Phi_t + \mathrm{Ro}(-\mathcal{J}(\psi_x, \Psi_z) + \mathcal{J}(\psi_z, \Psi_x) + \mathcal{J}(\psi, \nabla^2\Phi) + \mathcal{J}(\psi_x, \Phi_x) + \mathcal{J}(\psi_z, \Phi_z)) = 0, \tag{17c}$$

and the total energy becomes

$$\mathcal{E}_{\mathrm{tot}} = \int \frac{1}{2}(|\nabla\psi|^2 + |\nabla\Phi|^2 + |\nabla\Psi|^2)\mathrm{d}x\mathrm{d}z, \tag{18}$$

which consists of the kinetic energy of waves $\int |\nabla\psi|^2/2\ \mathrm{d}x\mathrm{d}z$, the potential energy of waves $\int |\nabla\Psi|^2/2\ \mathrm{d}x\mathrm{d}z$, and the energy of vortices $\int |\nabla\Phi|^2/2\ \mathrm{d}x\mathrm{d}z$.

B. Asymptotic expansion

We consider a rapidly rotating scenario with $\mathrm{Ro} \ll 1$, which leads to the dominant linear effect, and the nonlinear effects are of high order. So we introduce asymptotic expansions

$$\psi = \psi_0 + \mathrm{Ro}\psi_1 + \mathrm{Ro}^2\psi_2 + \cdots, \tag{19a}$$

$$\Psi = \Psi_0 + \mathrm{Ro}\Psi_1 + \mathrm{Ro}^2\Psi_2 + \cdots, \tag{19b}$$

$$\Phi = \Phi_0 + \mathrm{Ro}\Phi_1 + \mathrm{Ro}^2\Phi_2 + \cdots. \tag{19c}$$

To explore the rotating dominant scenario, we focus on the wave-dominant case, i.e., $\Phi_0 = 0$. Substituting the expansions (19) into the governing equations (17), we obtain equations of various orders of Ro.

At $O(1)$, we obtain

$$\partial_t\nabla^2\psi_0 - \nabla^2\Psi_0 = 0, \tag{20a}$$

$$\partial_t\nabla^2\Psi_0 + \nabla^2\psi_0 = 0. \tag{20b}$$

Whereafter, one obtains the leading-order solution

$$\psi_0 + \mathrm{i}\Psi_0 = A\mathrm{e}^{-\mathrm{i}t}, \tag{21}$$

where $A(x, z, \tau)$ is the wave amplitude, a complex function of slow time with $\tau = \mathrm{Ro}^2 t$. Here, the slow time is set to be $O(\mathrm{Ro}^2)$, which we explain below.

The $O(\mathrm{Ro})$ equations are

$$\nabla^2\psi_{1t} - \nabla^2\Psi_1 + \left(\frac{1}{4}\mathcal{J}(A, \nabla^2A)\mathrm{e}^{-2\mathrm{i}t} + \frac{1}{4}\mathcal{J}(A, \nabla^2A^*) + \mathrm{c.c.}\right) = 0, \tag{22a}$$

$$\nabla^2\Psi_{1t} + \nabla^2\psi_1 + \left(-\frac{\mathrm{i}}{4}\mathcal{J}(A, \nabla^2A)\mathrm{e}^{-2\mathrm{i}t} + \frac{\mathrm{i}}{4}\mathcal{J}(A, \nabla^2A^*) + \frac{\mathrm{i}}{4}\mathcal{J}(A_x, A_x^*) + \frac{\mathrm{i}}{4}\mathcal{J}(A_z, A_z^*) + \mathrm{c.c.}\right) = 0, \tag{22b}$$

$$\nabla^2\Phi_{1t} + \left(\frac{\mathrm{i}}{2}\mathcal{J}(A_x, A_z)\mathrm{e}^{-2\mathrm{i}t} + \mathrm{c.c.}\right) = 0, \tag{22c}$$

where c.c. denotes the complex conjugate. Equations (22) are solvable with solutions

$$\nabla^2\psi_1 = -\frac{\mathrm{i}}{4}\mathcal{J}(A, \nabla^2 A)\mathrm{e}^{-2\mathrm{i}t} - \frac{\mathrm{i}}{4}\boldsymbol{\nabla}\cdot\mathcal{J}(A, \boldsymbol{\nabla}A^*) + \text{c.c.}, \tag{23a}$$

$$\nabla^2\Psi_1 = -\frac{1}{4}\mathcal{J}(A, \nabla^2 A)\mathrm{e}^{-2\mathrm{i}t} + \frac{1}{4}\mathcal{J}(A, \nabla^2 A^*) + \text{c.c.}, \tag{23b}$$

$$\nabla^2\Phi_1 = \frac{1}{4}\mathcal{J}(A_x, A_z)\mathrm{e}^{-2\mathrm{i}t} + \text{c.c.} \tag{23c}$$

In this order, if we introduce a slow time $\tau' = \mathrm{Ro}t$, the first two equations in (22) would introduce a solvability condition of $A_{\tau'} = 0$, indicating a slower timescale.

At $O(\mathrm{Ro}^2)$, we obtain

$$\partial_t\nabla^2\psi_2 - \nabla^2\Psi_2 + \partial_\tau\nabla^2\psi_0 + \underbrace{\mathcal{J}(\psi, \nabla^2\psi)|_{0,1}}_{\mathcal{J}_1(A)\mathrm{e}^{-\mathrm{i}t}+\mathcal{J}_1(A)^*\mathrm{e}^{\mathrm{i}t}} = 0, \tag{24a}$$

$$\begin{aligned}&\partial_t\nabla^2\Psi_2 + \nabla^2\psi_2 + \partial_\tau\nabla^2\Psi_0 + \\ &\underbrace{(\mathcal{J}(\psi, \nabla^2\Psi) + \mathcal{J}(\psi_x, \Psi_x) + \mathcal{J}(\psi_z, \Psi_z) + \mathcal{J}(\psi_x, \Phi_z) - \mathcal{J}(\psi_z, \Phi_x))|_{0,1}}_{\mathcal{J}_2(A)\mathrm{e}^{-\mathrm{i}t}+\mathcal{J}_2(A)^*\mathrm{e}^{\mathrm{i}t}} = 0,\end{aligned} \tag{24b}$$

where the lower index $|_{0,1}$ denotes the interaction of $_0$ and $_1$ components in the quadratic terms, e.g., $\mathcal{J}(\psi, \nabla^2\psi)|_{0,1} = \mathcal{J}(\psi_1, \nabla^2\psi_0) + \mathcal{J}(\psi_0, \nabla^2\psi_1)$. We denote the sum of these terms in (a) and (b) as $\mathcal{J}_1(A)e^{-\mathrm{i}t} + \mathcal{J}_1(A)^*e^{\mathrm{i}t}$ and $\mathcal{J}_2(A)e^{-\mathrm{i}t} + \mathcal{J}_2(A)^*e^{\mathrm{i}t}$, respectively, as shown in the equations. Note that the equation for Φ_2 is solvable, but it is omitted in the above Eqs. (24).

Substituting the leading- and first-order solutions, (21) and (23), into Eqs. (24), and using $\mathcal{J}_1(A)\mathrm{e}^{-\mathrm{i}t} + \mathcal{J}_1(A)^*\mathrm{e}^{\mathrm{i}t}$ and $\mathcal{J}_2(A)\mathrm{e}^{-\mathrm{i}t} + \mathcal{J}_2(A)^*\mathrm{e}^{\mathrm{i}t}$ to denote cross terms in (24a) and (24b), respectively, we obtain

$$\partial_t\nabla^2\psi_2 - \nabla^2\Psi_2 + \left[\mathrm{e}^{-\mathrm{i}t}\left(\frac{1}{2}\nabla^2 A_\tau + \mathcal{J}_1(A)\right) + \text{c.c.}\right] = 0, \tag{25a}$$

$$\partial_t\nabla^2\Psi_2 + \nabla^2\psi_2 + \left[\mathrm{e}^{-\mathrm{i}t}\left(\frac{1}{2\mathrm{i}}\nabla^2 A_\tau + \mathcal{J}_2(A)\right) + \text{c.c.}\right] = 0. \tag{25b}$$

Multiplying Eq. (25b) by i and adding it to Eq. (25a), we obtain

$$\partial_t\nabla^2(\psi_2 + \mathrm{i}\Psi_2) + \mathrm{i}\nabla^2(\psi_2 + \mathrm{i}\Psi_2) + (\mathrm{e}^{-\mathrm{i}t}[\nabla^2 A_\tau + \mathcal{J}_1(A) + \mathrm{i}\mathcal{J}_2(A)] + \text{c.c.}) = 0. \tag{26}$$

The solvability condition for $\psi_2 + \mathrm{i}\Psi_2$ in Eq. (26) results in the equation for the slow evolution of wave amplitude $A(x, z, \tau)$:

$$\nabla^2 A_\tau + \frac{\mathrm{i}}{4}J_{\mathrm{NL}} = 0, \tag{27}$$

with

$$\begin{aligned}J_{\mathrm{NL}} = &-\mathcal{J}(A, \mathcal{J}(\boldsymbol{\nabla}A; \boldsymbol{\nabla}A^*)) \\ &+ \mathcal{J}(\boldsymbol{\nabla}A; \boldsymbol{\nabla}\Delta^{-1}\boldsymbol{\nabla}\cdot\mathcal{J}(A, \boldsymbol{\nabla}A^*)) - \mathcal{J}(\boldsymbol{\nabla}A^*; \boldsymbol{\nabla}\Delta^{-1}\mathcal{J}\big(A, \nabla^2 A\big)) \\ &+ \tfrac{1}{2}\mathcal{J}(A_x^*, \partial_z[\Delta^{-1}\mathcal{J}(A_x, A_z)]) - \tfrac{1}{2}\mathcal{J}(A_z^*, \partial_x[\Delta^{-1}\mathcal{J}(A_x, A_z)]),\end{aligned} \tag{28}$$

where $\mathcal{J}(\boldsymbol{\nabla}a; \boldsymbol{\nabla}b) = \mathcal{J}(a_x, b_x) + \mathcal{J}(a_z, b_z)$, and Δ^{-1} is the inverse of the Laplacian operator. The nonlinear terms show that wave quartic interaction controls the slow dynamics, which is also a corollary of the dispersion relation $\omega = \pm 1$. It is special that all nonlinear terms in the above amplitude equation contain the Jacobian operator, therefore a one-dimensional correspondence of the current system is not possible because an x (or z) -independent solution has no nonlinear effect. This form distinguishes it from other wave systems such as the MMT system [36].

Multiplying Eq. (27) by A^*, adding the conjugate of the resultant equation, and integrating over space with doubly periodic boundary conditions, we obtain the energy conservation

$$\partial_\tau \int \nabla A \cdot \nabla A^* \mathrm{d}x\mathrm{d}z = 0. \tag{29}$$

Note that at the leading order $\Phi_0 = 0$, the vortex energy $\int |\nabla\Phi|^2/2\ \mathrm{d}x\mathrm{d}z$ is of high order. Thus, the total energy (18) is approximated as

$$\begin{aligned}\mathcal{E}_{\mathrm{tot}} &= \int \frac{1}{2}(|\nabla\psi|^2 + |\nabla\Psi|^2)\mathrm{d}x\mathrm{d}z\\ &\approx \int \frac{1}{2}(|\nabla\psi_0|^2 + |\nabla\Psi_0|^2)\mathrm{d}x\mathrm{d}z = \int \frac{1}{2}|\nabla A|^2\mathrm{d}x\mathrm{d}z \equiv \mathcal{E}_A.\end{aligned} \tag{30}$$

Since Ro could be scale-dependent, we need to think about the scales that enable our asymptotic expansion. Equation (27) in its dimensional form can be written as

$$\tilde{\nabla}^2\tilde{A}_{\tilde{\tau}} + \frac{fL^2}{U^2}\frac{\mathrm{i}}{4}\tilde{J}_{\mathrm{NL}} = 0, \tag{31}$$

where the tilde symbol is used to denote the dimensional form of the terms. Then the energy injection rate $\epsilon \sim (fL^2/U^2)\tilde{A}\tilde{J}_{\mathrm{NL}} \sim fU^2$. Using the Zeman scale, where the characteristic scale of inertial wave and eddy turnover time are equal, $L_Z \sim \epsilon^{1/2}f^{-3/2}$, we obtain $\mathrm{Ro} \sim U/fL \sim \epsilon^{1/2}f^{-3/2}L^{-1} \sim L_Z/L$. Thus, our asymptotic expansion based on $\mathrm{Ro} \ll 1$ works for scales much larger than the Zeman scale.

C. Energy spectrum

We can obtain the wave energy spectrum from the nonlinear wave amplitude equation (27). Since the quartic interaction with constant frequency does not rule out any interacting modes, which happens in dispersive wave turbulence, we follow the strong turbulence argument (cf. [37]). Denoting L as a lengthscale, the nonlinear terms of wave amplitude equation (27) scale as, e.g.,

$$J_{\mathrm{NL}} \sim \mathcal{J}(A, \mathcal{J}(\nabla A; \nabla A^*)) \sim A^3/L^6, \tag{32}$$

and the other nonlinear terms have the same dimension. Thus, the strong turbulence implies that the energy flux scales as $AJ_{\mathrm{NL}} \sim A^4/L^6$. Considering Kolmogorov's constant-flux picture, we have $A^4/L^6 = \mathrm{const}$, i.e., $A \sim L^{3/2}$. Since

$$\int E(K)\mathrm{d}K = \frac{\int |\nabla A|^2 \mathrm{d}\boldsymbol{x}}{\int \mathrm{d}\boldsymbol{x}}, \tag{33}$$

where $K = \sqrt{k^2 + m^2}$, the energy spectrum follows

$$E(K) \sim K^{-2}, \tag{34}$$

which is consistent with the result of Zeman [20] and Zhou [21]. Note that this expression of the spectrum works when $K \ll K_Z$. Additionally, we notice that, as mentioned in our hypothesis, linear waves dominate this system, therefore we may use wave turbulence theory to study this problem, which we discuss in Appendix B.

IV. NUMERICAL SIMULATIONS

We performed forcing-dissipative numerical simulations of both the amplitude equation (27) and original Eqs. (5) with zero initial state. The simulations are performed in a box of size $2\pi \times 2\pi$ with a resolution 512×512. We use a Fourier pseudospectral method with 1/2 dealiasing for the amplitude equation and 2/3 dealiasing for original equations in space, and a fourth-order explicit Runge-Kutta scheme in time.

Xie and Bühler [34] showed a forward energy cascade in the original system (5). Therefore, we can exert force from the very first wave number. The white-noise forcing term, which we will specify in Eqs. (38) and (40) below, is prescribed in the Fourier space by

$$F = \mathrm{Re}\{\mathcal{F}^{-1}\{\hat{F}\}\} \quad \text{with} \quad \hat{F} = M_F H(K_f - K)\mathcal{A}\mathrm{e}^{\mathrm{i}2\pi\mathcal{B}}, \tag{35}$$

where M_F is the magnitude of forcing, H is the Heaviside function, $\mathcal{A}$ is a Gaussian random variable, and $\mathcal{B}$ follows a uniform distribution. To ensure enough wave nonlinear interaction, the forcing acts in a wide range $[1,\ K_f]$ in the wave-number space.

Following [38], we choose an exponential cutoff filter for dissipation,

$$H_{\mathrm{ec}}(K) = \begin{cases} \exp(-a(K - K_{\mathrm{cut}})^s), & K > K_{\mathrm{cut}}, \\ 1, & K \leqslant K_{\mathrm{cut}}, \end{cases} \tag{36}$$

where

$$a = \frac{\ln{(1 + 4\pi/N)}}{(K_{\max} - K_{\mathrm{cut}})^s}. \tag{37}$$

Here N is the resolution, $K_{\max}$ is the maximum wave number, K_{cut} is the cutoff wave number, and s, which we choose to be 2, is a parameter describing the order of a corresponding hyperviscosity filter. This filter acts on the equation via $\hat{\psi}_n = \hat{\psi}_n' H_{\mathrm{ec}}(K)$, where $\hat{\psi}_n'$ is the Fourier transform of ψ calculated by the nondissipative equation at the nth time step. This process can be replaced by a pseudodissipative term (cf. [38]) $D\psi$ added to the right-hand side of the equation. Since there is no dissipation at wave numbers smaller than the cutoff wave number, K_{cut}, we can obtain a range in the wave-number space with a constant energy flux.

A. The amplitude equation

In this section, we show the numerical results of the amplitude equation (27). With forcing and dissipation, the equation becomes

$$\nabla^2 A_\tau = -\frac{\mathrm{i}}{4} J_{\mathrm{NL}} + \mathcal{F}^{-1}\{\hat{F}\} + DA, \tag{38}$$

where F is the forcing with $K_f = 4$, $M_F = 400$ [cf. (35)], and energy injection rate $\epsilon = 2.3 \times 10^{-6}$, and D is the equivalent form of exponential cutoff dissipation with $K_{\mathrm{cut}} = 160$.

The evolution of total energy $\mathcal{E}_A = \int \nabla A \cdot \nabla A^*/2\, \mathrm{d}x\mathrm{d}z$ reaches the statistically steady phase around $\tau = 7000$, and the statistical quantities are calculated among ($\tau \in [7000,\ 8000]$). Figure 1(a) shows the energy spectrum $E_A(K)$, where the notation of E denotes the energy spectrum, and for a given field χ, $\int E_\chi(K)\mathrm{d}K = \int \nabla\chi \cdot \nabla\chi^*/2\, \mathrm{d}x\mathrm{d}z$. The spectrum approximately proportional to K^{-2} in the range $K \in [4, 50]$ and $K^{1/2}$ in the range $K \in [60, 160]$.

We calculate the total energy flux by

$$F_A(K) = \int_0^K \int_0^{2\pi} \frac{1}{2}\left(-\frac{\mathrm{i}}{4}\hat{A}^*\widehat{J_{\mathrm{NL}}} + \mathrm{c.c.}\right)\kappa\, \mathrm{d}\kappa\, \mathrm{d}\alpha, \tag{39}$$

where $\hat{\cdot}$ denotes the Fourier transform, and we show total energy flux in Fig. 1(b). We observe an inertial range of constant energy flux between the forcing wave number $K_f = 4$ and the dissipation wave number $K_{\mathrm{cut}} = 160$. The existence of the inertial range and the K^{-2} energy spectrum aligns with our deduction in Sec. III C. Concerning the "bottleneck" range $K \in [60, 160]$ in Fig. 1(a), since a wave system usually has two statistically steady solutions, corresponding to the Kolmogorov-Zakharov spectrum and the thermal equilibrium spectrum, respectively [27], the $K^{1/2}$ scaling could be a combination of the Kolmogorov-Zakharov spectrum and the Rayleigh-Jeans spectrum, K^1, in the 2D case. Using the spectrum of E_A and Eqs. (21) and (23), we can deduce by dimensional analysis the spectra of $O(\mathrm{Ro})$ terms, which we discuss in Appendix A 1.

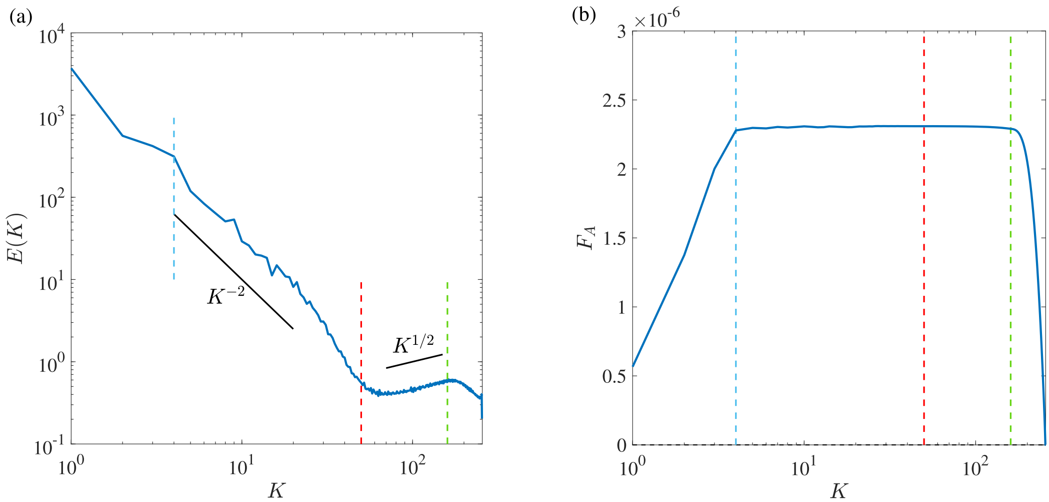

FIG. 1. Energy spectrum $E_A(K)$ (a) and energy flux (b) (positive means downscale) averaged over $\tau \in [7100, 7900]$ of the simulation with $K_f = 4$ and $\epsilon = 2.3 \times 10^{-6}$. The blue, red, and green dashed lines mark $K_f = 4$, $K = 50$, and $K_{\text{cut}} = 160$, respectively. The two solid black lines are references for K^{-2} and $K^{1/2}$.

B. The original equations

In this section, we perform numerical simulations of the original Eqs. (5). Here, we emphasize that the forcing is only exerted on the ψ Eq. (5a) to avoid the direct excitation of the vortical part [cf. (12)]. With forcing and dissipation, the equations become

$$\nabla^2\psi_t + \mathcal{J}(\psi, \nabla^2\psi) - \theta_x + v_z = F + D\psi, \tag{40a}$$

$$v_t + \mathcal{J}(\psi, v) - \psi_z = Dv, \tag{40b}$$

$$\theta_t + \mathcal{J}(\psi, \theta) + \psi_x = D\theta, \tag{40c}$$

where F is the forcing with $K_f = 4$, $M_F = 3$ [cf. (35)], and D is the equivalent form of exponential cutoff dissipation with $K_{\text{cut}} = 150$.

Note that we omit Ro in the nonlinear terms. As is discussed in Sec. III B, Ro $\ll 1$ is equivalent to $K \ll K_Z$ here. Therefore, in the current simulation, we design K_Z to be much bigger than the wave numbers in the inertial range to guarantee the rapidly rotating turbulence by choosing proper values of M_F.

In the current simulation, the total energy injection rate is $\epsilon = 1.1 \times 10^{-8}$ and the corresponding Zeman wave number is $K_Z = \epsilon^{-1/2} f^{3/2} \approx 9.4 \times 10^3$ (here $f = 1$ due to our rescaling), which is much larger than K_{cut} and ensures the dominance of linear waves and a rapidly rotating turbulence.

We plot in Fig. 2 the evolution of wave kinetic energy $\mathcal{E}_\psi = \int |\nabla\psi|^2/2 \, \mathrm{d}x\mathrm{d}z$, wave potential energy $\mathcal{E}_\Psi = \int |\nabla\Psi|^2/2 \, \mathrm{d}x\mathrm{d}z$, and the vortical energy $\mathcal{E}_\Phi = \int |\nabla\Phi|^2/2 \, \mathrm{d}x\mathrm{d}z$, which is of high order in the current setup. As expected, the vortical energy is far less than that of waves, justifying that our simulation is a good realization of a wave-dominant system. Potential and kinetic energies fluctuate strongly and rapidly because we consider a wave-dominant system where potential and kinetic energy transfers. As shown in the zoomed-in figure of Fig. 2, a dominant timescale of energy fluctuation is around π, which is one-half of the wave period 2π due to the quadratic energy.

We show energy spectra and energy fluxes in Fig. 3, where the fluxes are defined by

$$F_\Psi(K) = \int_0^K \int_0^{2\pi} \frac{1}{2}(\hat{\Psi}^* \hat{N_\Psi} + \text{c.c.})\kappa \, \mathrm{d}\kappa \, \mathrm{d}\alpha, \quad N_\Psi = \partial_x \mathcal{J}(\psi, \theta) - \partial_z \mathcal{J}(\psi, v), \tag{41a}$$

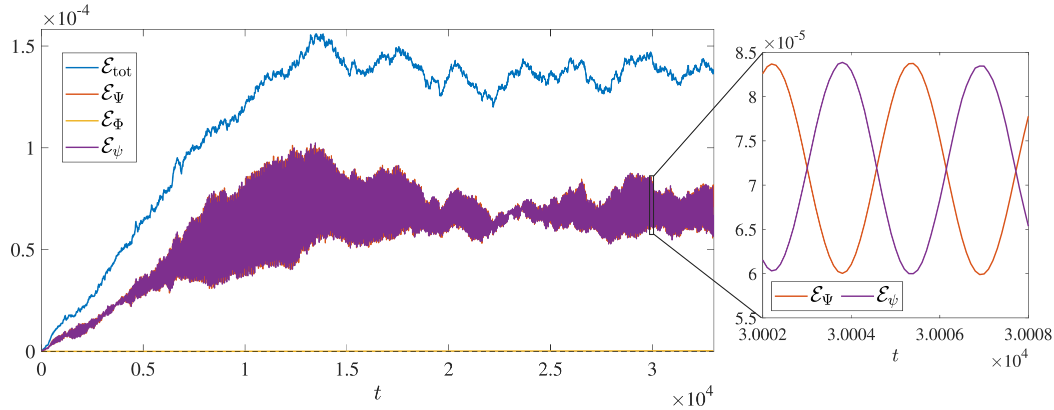

FIG. 2. Evolution of wave kinetic energy $\mathcal{E}_\psi$, wave potential energy $\mathcal{E}_\Phi$, vortical energy $\mathcal{E}_\psi$, and total energy $\mathcal{E}_{\rm tot} = \mathcal{E}_\psi + \mathcal{E}_\Psi + \mathcal{E}_\Phi$ of the simulation with $K_f = 4$ and $\epsilon = 1.1 \times 10^{-8}$. Right: detailed view of the wave energy.

$$F_\Phi(K) = \int_0^K \int_0^{2\pi} \frac{1}{2}(\hat{\Phi}^* \hat{N_\Phi} + \text{c.c.})\kappa \, d\kappa \, d\alpha, \quad N_\Phi = \partial_z \mathcal{J}(\psi, \theta) + \partial_x \mathcal{J}(\psi, v), \tag{41b}$$

$$F_\psi(K) = \int_0^K \int_0^{2\pi} \frac{1}{2}(\hat{\psi}^* \hat{N_\psi} + \text{c.c.})\kappa \, d\kappa \, d\alpha, \quad N_\psi = -\mathcal{J}(\psi, \nabla^2 \psi), \tag{41c}$$

$$F_{\rm tot}(K) = F_\Psi(K) + F_\Phi(K) + F_\psi(K). \tag{41d}$$

We observe an inertial range $K \in [4, 40]$ and a corresponding K^{-2} spectrum. The overlapping of curves of E_Ψ and E_ψ shows the linear wave dominance. Also, we find an approximate K^0 scaling of the energy spectrum in the range with $K \in [40, 150]$, which could be a combination of

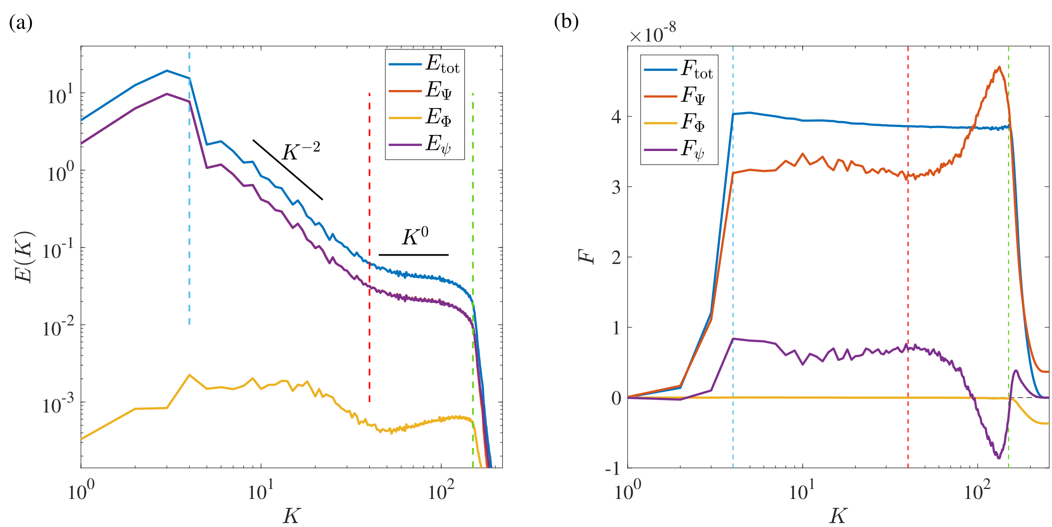

FIG. 3. Energy spectrum (a) and energy flux (b) of the simulation with $K_f = 4$ and $\epsilon = 1.1 \times 10^{-8}$. The two solid black lines are K^{-2} and K^0 as references. The blue, red, and green dashed lines mark $K_f = 4$, $K = 40$, and $K_{\rm cut} = 150$, respectively. $F_{\rm tot}$ is the energy flux of total energy, and F_Ψ, F_Φ, F_ψ are the corresponding energy flux of E_Ψ, E_Φ, and E_ψ, respectively.

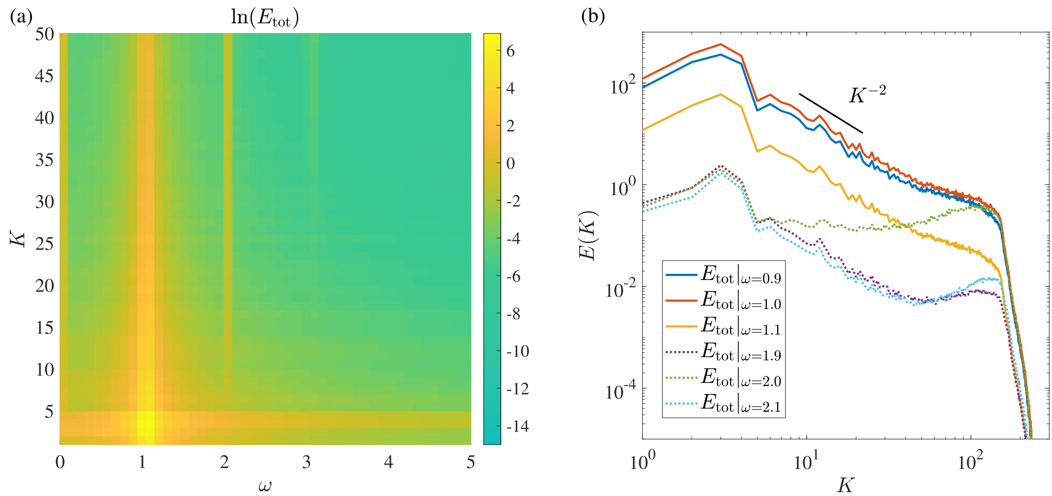

FIG. 4. (a) The total spatial-temporal Fourier spectrum. (b) Spectra of total energy at different ω are plotted. The solid black line is K^{-2}.

the Kolmogorov-Zakharov spectrum and the Rayleigh-Jeans spectrum. These results are consistent with those of the amplitude equation in Sec. IV A. As for the differences in the higher wave-number region $K > 50$, considering that the amplitude equation is asymptotically obtained under the small Rossby number limit, the expansion requires the nonlinear term to be much smaller compared with the Coriolis term, but the relative sizes of these two terms are scale-dependent. Using the ad hoc scaling $A \sim L^{3/2}$, the scale-dependent Rossby number scales as $A/L^2 \sim L^{-1/2}$, which implies that for a given parameter set, the expansion works better at large scales than small scales. Moreover, the bottleneck effect could be different for the two systems. These cause the differences between the two simulations, especially in the higher wave-number region $K > 50$.

The spatial-temporal spectrum shown in Fig. 4(a) also justifies the weakly nonlinear character. The total energy E_{tot} centers along the linear dispersion relation $\omega = \pm 1$, and the energy concentration along $\omega = 2$ and 0 is in accordance with the wave quartic interaction. The energy concentration in the range $K \in [1, 4]$ is a result of forcing. The energy spectra at different frequencies ω are shown in Fig. 4(b). Almost all the spectra scale as K^{-2}, while at $\omega = 2.0$, $E_{\mathrm{tot}}|_{\omega=2} \sim K^0$. Notably, $E_{\mathrm{tot}}|_{\omega=2}$ is $O(\mathrm{Ro})$ and we discuss $O(\mathrm{Ro})$ terms in Appendix A 2.

C. The classic (anisotropic) 2D rotating turbulence

As a comparison, we perform a simulation of the classic anisotropic 2D rotating turbulence, whose governing equations are

$$\nabla^2\psi_t + \mathcal{J}(\psi, \nabla^2\psi) + v_z = F^G + D\psi + \alpha\nabla^2\psi, \tag{42a}$$

$$v_t + \mathcal{J}(\psi, v) - \psi_z = Dv + \alpha\nabla^2 v, \tag{42b}$$

where F^G is a Gaussian forcing,

$$F^G = \mathrm{Re}\{\mathcal{F}^{-1}\{\hat{F}^G\}\} \quad \text{with} \quad \hat{F}^G = M_F \mathrm{e}^{-\frac{(K-K_f)^2}{2D_K^2}} \mathcal{A} \mathrm{e}^{\mathrm{i}2\pi\mathcal{B}}, \tag{43}$$

$M_F = 3$, $K_f = 6$, $D_K = 2$, and D is the equivalent form of exponential cutoff dissipation with $K_{\mathrm{cut}} = 150$. The last terms on the right-hand side (r.h.s.) are extra damping terms at large scales with $\alpha = 0.1$. Note that the simulation of this anisotropic system has different parameters from the previous one of the isotropic system in Sec. IV B. Like two-dimensional Rayleigh-Bénard convection, it

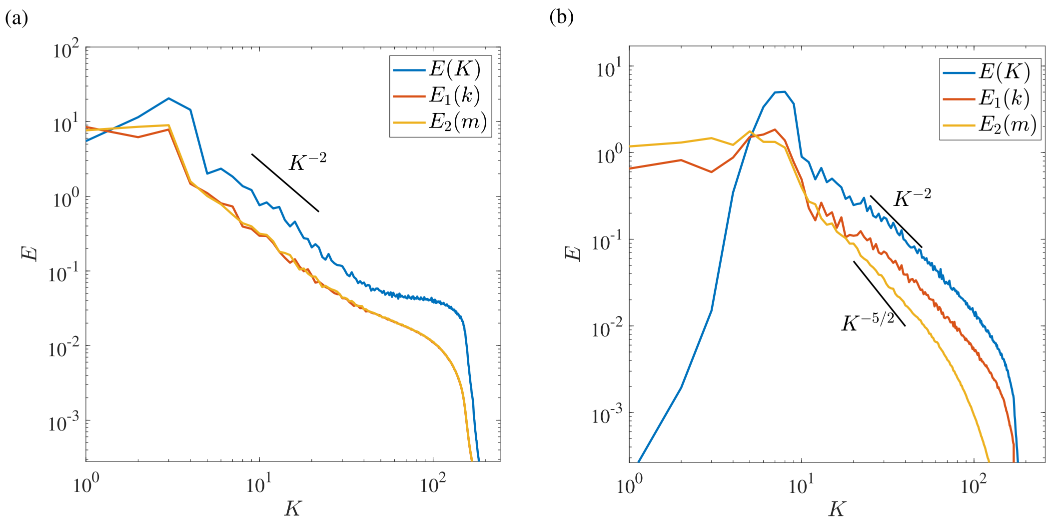

FIG. 5. Energy spectra along different orientations. $E_1(k) = \sum_m E(k, m)$ along the k axis, $E_2(m) = \sum_k E(k, m)$ along the m axis. (a) The simulation of the original isotropic system (5). (b) The simulation of the anisotropic system (42).

is inevitable that this anisotropic system will reach a statistically steady state without large-scale coherent structures, and we need a large-scale dissipative term to saturate the inverse cascade when present (cf. Winchester *et al.,* [39]). So, to avoid this energy accumulation, we change the forcing term and add an extra damping term at large scales. This system (42) has a dispersion relation $\omega = \pm m/K \in [0,\ 1]$, which implies a wide range of characteristic timescales. When $m \to 0$ with fixed k, $\omega \to 0$ and therefore $t_{\text{wave}} = 1/\omega \gg t_{\text{NL}} = \epsilon^{-1/3}K^{-2/3}$, which implies the dominance of nonlinear effects, and hence like a $beta$-plane turbulence [40] energy tends to accumulate at large scale around $m = 0$. Since the new forcing and extra damping are isotropic, they do not directly introduce anisotropic effects to the system (42), and the observed anisotropy should be the effect of the system itself.

Figure 5 compares energy spectra along different orientations in the isotropic and anisotropic systems. Here, $E_1(k) = \sum_m E(k, m)$ and $E_2(m) = \sum_k E(k, m)$, where $\sum_m$ and $\sum_k$ mean the summation over all wave numbers m and k, respectively. In the isotropic system, the curves of $E_1(k)$ and $E_2(m)$ align closely with the same K^{-2} scaling, while in the anisotropic system, the two separate from each other, with $E_1(k)$ scaling as K^{-2} and $E_2(m)$ scaling as $K^{-5/2}$.

We examine second-order structure functions $\overline{\delta u^2 + \delta w^2}$, which measure accumulated energy, and third-order structure functions, e.g., $\nabla \cdot V_K = \nabla \cdot \overline{\delta \boldsymbol{u}(\delta u^2 + \delta w^2)}$, $\nabla \cdot V_P = \nabla \cdot \overline{\delta \boldsymbol{u}(\delta \theta^2 + \delta v^2)}$, and $\nabla \cdot V = \nabla \cdot V_K + \nabla \cdot V_P$, which measure energy flux, to provide further verification of isotropy. Figures 6 and 7 show the fields of second- and third-order structure functions of the two systems. Note that the square computation domain causes the anisotropy at large scales of the isotropic system, and the flocculent structures or narrow cones are the results of resonant wave interactions at very small K close to the forcing scales (cf. [41]). As the anisotropic system, vertical bands appear in Fig. 6(b). As discussed above, energy accumulates at large scales around $m = 0$, thus z-direction bands appear.

V. SUMMARY AND DISCUSSION

We study the validity of the isotropic arguments in an artificial isotropic rotating fluid system. In the wave-dominant scenario, i.e., Ro $\ll 1$, the linear inertial wave has a single timescale, so this system is a perfect example that agrees with the assumptions by Zeman [20] and Zhou [21]

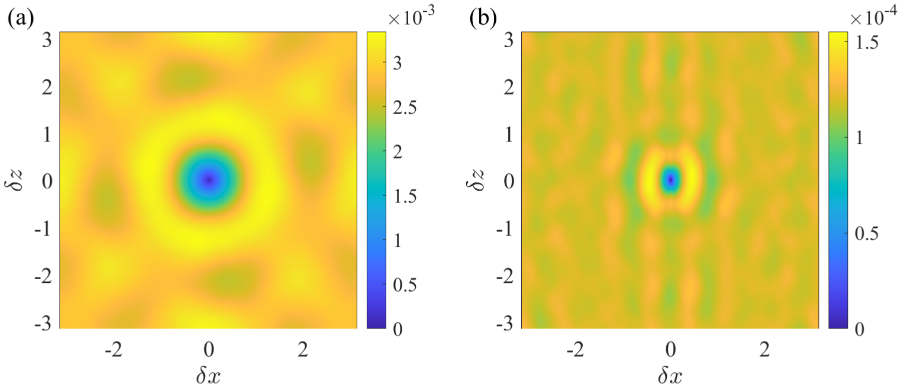

FIG. 6. Second-order structure function $\overline{\delta u^2 + \delta w^2}$ of the isotropic system (5) (a) and the anisotropic system (42) (b).

to obtain the K^{-2} energy spectrum for rotating turbulence. We asymptotically derive an amplitude equation for the slow evolution of the wave amplitude and obtain the K^{-2} energy spectrum using the strong turbulence argument based on a constant downscale energy flux. The statistical isotropy and the K^{-2} scaling are justified in numerical simulations of both the amplitude equation and the isotropic rotating system. As a comparison, in an anisotropic 2D rotating system, energy spectra have different scalings along different directions.

Weak wave turbulence theory can also obtain the K^{-2} spectrum in the context of Zeman's and Zhou's discussions (cf. Appendix B). Notably, wave turbulence theory generally handles resonant interaction of weak dispersive waves. However, considering the dispersion relation $\omega = \pm f$ where the frequency is independent of wave number in the current isotropic rotating system, the quartic interaction does not rule out any interacting modes, such as what happens in dispersive wave turbulence. The dispersion relation also implies a zero group velocity, which leads to a strong turbulence argument, which differs from the weak wave turbulence.

This study provides a theoretical approach to fill the gap between realistic anisotropic systems and isotropic theories. Practically, we may realize the current 2D isotropic rotating system in experiments by confining the rotating stratified flow between two vertically oriented parallel plates or employing a magnetic field to restrict the flow.

ACKNOWLEDGMENTS

This work has received financial support from the National Natural Science Foundation of China (NSFC) under Grants No. 12272006, No. 42361144844 and No. 12472219, and from the Laoshan Laboratory under Grants No. SKJ202202000 and No. LSKJ202300100.

APPENDIX A: THE FIRST-ORDER TERMS IN SIMULATIONS

1. The amplitude equation

Now that the spectrum of E_A scales as K^{-2}, which implies $A \sim K^{-3/2}$, we can deduce by dimensional analysis as in Sec. III C from (21) and (23) that the spectra of leading terms $E_{\psi 0}$ and $E_{\Psi 0}$ should scale as K^{-2}, and the spectra of order-1 terms $E_{\psi 1}$, $E_{\Psi 1}$, and $E_{\Phi 1}$ should scale as K^{-1}. For example, substituting $A \sim K^{-3/2}$ into Eq. (23a), we obtain $\psi_1 \sim K^{-1}$, and then considering $E_{\psi 1}\mathrm{d}K \sim \nabla\psi_1 \cdot \nabla\psi_1^*$, we get $E_{\psi 1} \sim K^{-1}$. We numerically calculate the corresponding spectra of ψ_0, Ψ_0, ψ_1, Ψ_1, and Φ_1 in Fig. 8. The results are in agreement with our asymptotic calculation. We then plot the fields of time-averaged spectra in Fig. 9 to show the isotropy again.

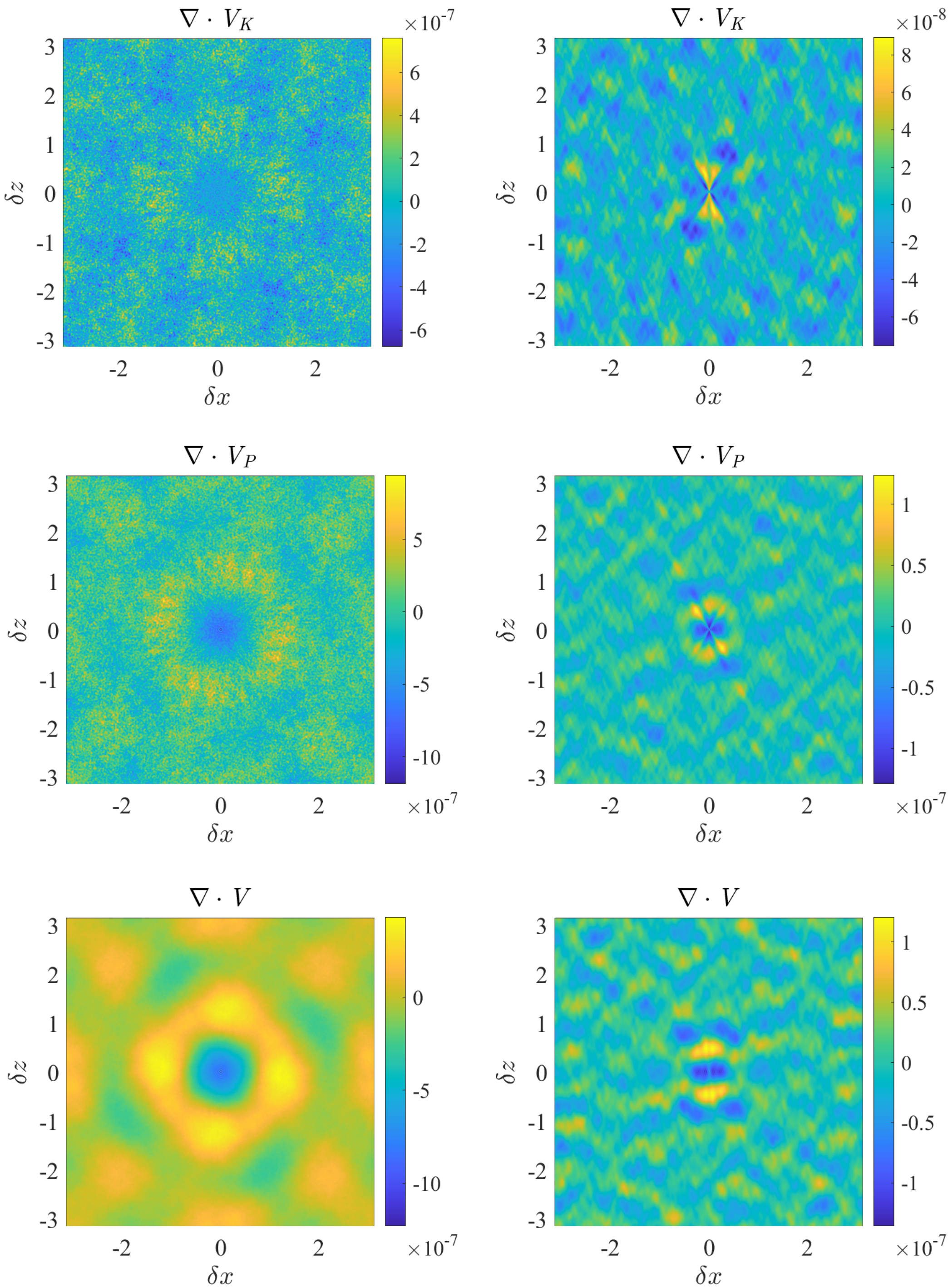

FIG. 7. Third-order structure functions $\nabla \cdot V_K = \nabla \cdot \overline{\delta \boldsymbol{u}(\delta u^2 + \delta w^2)}$, $\nabla \cdot V_P = \nabla \cdot \overline{\delta \boldsymbol{u}(\delta \theta^2 + \delta v^2)}$, and $\nabla \cdot V = \nabla \cdot V_K + \nabla \cdot V_P$ of the isotropic system (5) (left column) and the anisotropic system (42) (right column).

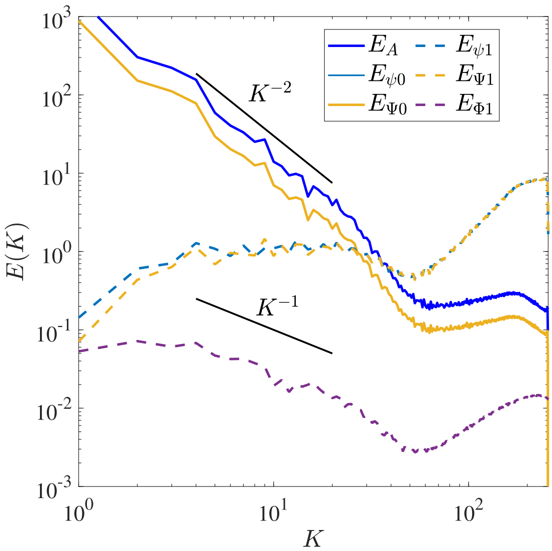

FIG. 8. Plot of E_A, $E_{\psi0}$, $E_{\Psi0}$, $E_{\psi1}$, $E_{\Psi1}$, and $E_{\Phi1}$. The two solid black lines in the figure are references for K^{-2} and K^{-1}.

2. The original equations

From (21) and (23) we calculate the spectra of $O(1)$ terms and show them in Fig. 10, where we approximate ψ_0 as ψ and Ψ_0 as Ψ. The results are similar to Fig. 8 of the simulation of the amplitude equation.

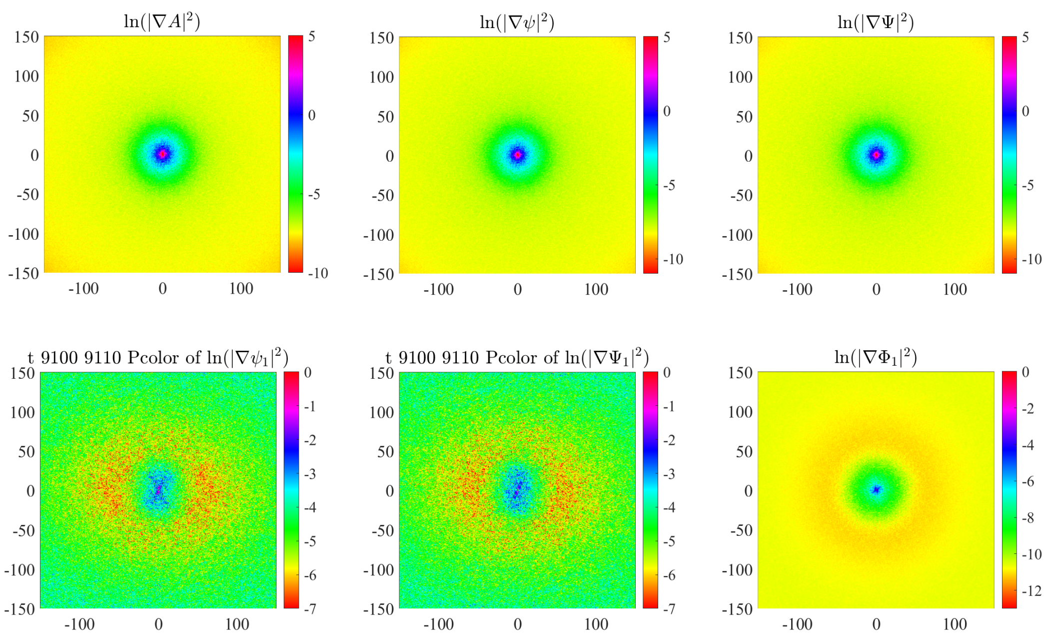

FIG. 9. Fields of $|\nabla A|^2$, $|\nabla\psi|^2$, $|\nabla\Psi|^2$, $|\nabla\psi_1|^2$, $|\nabla\Psi_1|^2$, $|\nabla\Phi_1|^2$, averaged over $t \in [7100, 7900]$. The horizontal axis is the k-axis and the vertical axis is the m-axis.

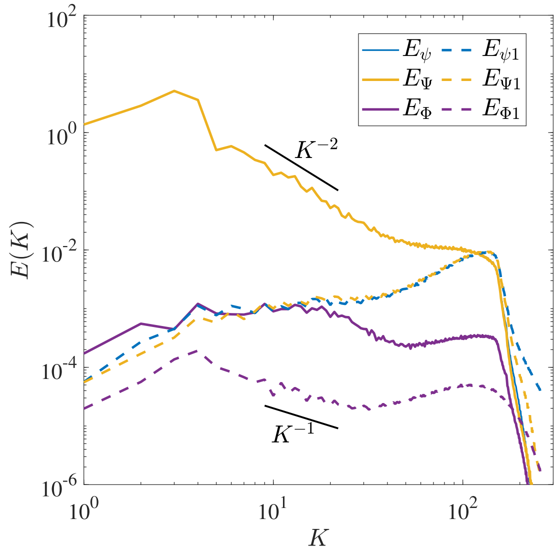

FIG. 10. Energy spectra E_A, $E_{\psi 0}$, $E_{\Psi 0}$, $E_{\psi 1}$, $E_{\Psi 1}$, and $E_{\Phi 1}$. The two solid black lines are K^{-2} and K^{-1} as references.

Since the $O(\mathrm{Ro})$ terms are terms with $\omega = 2$ and 0 [cf. (23)], the behaviors of the spectra of ψ_1 and Ψ_1 in Fig. 10 and $E_{\mathrm{tot}}|_{w=2.0}$ in Fig. 4(b) are consistent. However, $E_{\psi 1}$ and $E_{\Psi 1}$ (and $E_{\mathrm{tot}}|_{w=2.0}$) should scale as K^{-1} [cf. (23)], rather than K^0 in Figs. 4(b), 10, and 8. We guess that the phase distribution of the amplitude is not uniform enough to support our dimensional analysis for order-1 terms. Also, we plot the fields of time-averaged spectra in Fig. 11. The anisotropy of $|\nabla\psi_1|^2$

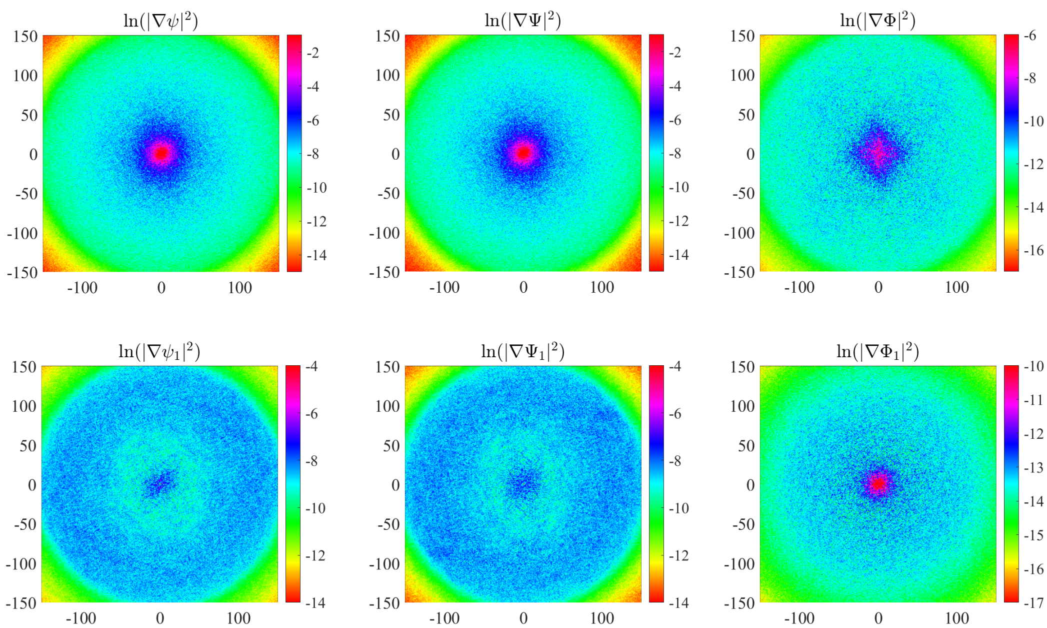

FIG. 11. Fields of $|\nabla\psi|^2$, $|\nabla\Psi|^2$, $|\nabla\Phi|^2$, $|\nabla\psi_1|^2$, $|\nabla\Psi_1|^2$, $|\nabla\Phi_1|^2$. The horizontal axis is the k-axis and the vertical axis is the m-axis.

and $|\nabla\Psi_1|^2$ shows that ψ_1 and Ψ_1 have nonuniform phase distributions, implying that the phase distribution of the amplitude is not uniform enough, which supports our guess. In addition, the field of $|\nabla\Phi|^2$ is also anisotropic but seems to be a square, which could be caused by the square computation domain.

APPENDIX B: SCALINGS OF THE ENERGY SPECTRUM OBTAINED BY WAVE TURBULENCE THEORY

Dimensional analysis in WT theory [27] shows that for general d-dimensional wave systems, the energy cascade spectrum has the scaling

$$E_K^{(1\mathrm{D})} \sim \lambda^x \epsilon^{1/(N-1)} K^y,$$

where

$$x = 2 - \frac{3}{N-1}, \qquad y = d - 6 + 2\alpha + \frac{5-d-3\alpha}{N-1},$$

N is the minimal number of resonant waves, ϵ is the energy injection rate, and λ and α come from the dispersion relation $\omega = \lambda K^\alpha$.

In classic 3D anisotropic rotating turbulence, the dispersion relation is

$$\omega = f\frac{k_\parallel}{K}$$

($\parallel$ refers to the rotation axis). If we consider an isotropic assumption that $k_\parallel \sim k_\perp$, we can take $\lambda \sim f$ and $\alpha = 0$. With $d = 3$ and $N = 3$, we get [27]

$$E_K^{(1\mathrm{D})} \sim f^{1/2}\epsilon^{1/2}K^{-2}.$$

Thus WT theory also gives a K^{-2} spectrum for 3D rotating turbulence, which is consistent with Zeman [20] and Zhou [21] in the 3D condition.

However, in our 2D system where the dispersion relation is $\omega = \pm f$, in the WT spectrum we should take $\lambda = 1$, $\alpha = 0$, $d = 2$, and $N = 4$, and we obtain

$$E_K^{(1\mathrm{D})} \sim f\epsilon^{1/3}K^{-3},$$

which differs from K^{-2}. Notably, wave turbulence theory generally handles the resonant interaction of dispersive waves. However, in our current system, considering the nondispersive dispersion relation $\omega = \pm f$, the quartic interaction is nontrivial, making the limit of $\alpha \to 0$ in WT singular. The dispersion relation also implies a zero group velocity, which leads to a strong turbulence argument differing from weak wave turbulence. Thus, whether the WT theory applies to $\alpha = 0$ cases remains an open question.

[1] R. Salmon, *Lectures on Geophysical Fluid Dynamics* (Oxford University Press, USA, 1998).

[2] G. K. Vallis, *Essentials of Atmospheric and Oceanic Dynamics* (Cambridge University Press, Cambridge, 2019).

[3] J. Marshall and R. A. Plumb, *Atmosphere, Ocean, and Climate Dynamics: An Introductory Text*, International Geophysics Series Vol. 93 (Elsevier Academic, Amsterdam, 2008).

[4] R. E. Mayne, The role of laminar-turbulent transition in gas turbine engines, J. Turbomach. **113**, 509 (1991).

[5] E. Deusebio, G. Boffetta, E. Lindborg, and S. Musacchio, Dimensional transition in rotating turbulence, Phys. Rev. E **90**, 023005 (2014).

[6] P. A. Davidson, *Turbulence: An Introduction for Scientists and Engineers* (Oxford University Press, Oxford, 2015).
[7] B. Gallet, Exact two-dimensionalization of rapidly rotating large-reynolds-number flows, J. Fluid Mech. **783**, 412 (2015).
[8] R. H. Kraichnan, Inertial ranges in two-dimensional turbulence, Phys. Fluids **10**, 1417 (1967).
[9] L. M. Smith, J. R. Chasnov, and F. Waleffe, Crossover from two- to three-dimensional turbulence, Phys. Rev. Lett. **77**, 2467 (1996).
[10] J. Cho, Forward and inverse cascades in EMHD turbulence, J. Phys.: Conf. Ser. **719**, 012001 (2016).
[11] M. K. Sharma, M. K. Verma, and S. Chakraborty, On the energy spectrum of rapidly rotating forced turbulence, Phys. Fluids **30**, 115102 (2018).
[12] M. K. Sharma, M. K. Verma, and S. Chakraborty, Anisotropic energy transfers in rapidly rotating turbulence, Phys. Fluids **31**, 085117 (2019).
[13] L. M. Smithr and V. Yakhot, Finite-size effects in forced two-dimensional turbulence, J. Fluid Mech. **274**, 115 (1994).
[14] J. Y. N. Cho and E. Lindborg, Horizontal velocity structure functions in the upper troposphere and lower stratosphere: 1. Observations, J. Geophys. Res.: Atmos. **106**, 10223 (2001).
[15] M. G. Shats, H. Xia, H. Punzmann, and G. Falkovich, Suppression of turbulence by self-generated and imposed mean flows, Phys. Rev. Lett. **99**, 164502 (2007).
[16] A. M. Rubio, K. Julien, E. Knobloch, and J. B. Weiss, Upscale energy transfer in three-dimensional rapidly rotating turbulent convection, Phys. Rev. Lett. **112**, 144501 (2014).
[17] R. Marino, A. Pouquet, and D. Rosenberg, Resolving the paradox of oceanic large-scale balance and small-scale mixing, Phys. Rev. Lett. **114**, 114504 (2015).
[18] A. van Kan and A. Alexakis, Energy cascades in rapidly rotating and stratified turbulence within elongated domains, J. Fluid Mech. **933**, A11 (2022).
[19] D. Balwada, J.-H. Xie, R. Marino, and F. Feraco, Direct observational evidence of an oceanic dual kinetic energy cascade and its seasonality, Sci. Adv. **8**, eabq2566 (2022).
[20] O. Zeman, A note on the spectra and decay of rotating homogeneous turbulence, Phys. Fluids **6**, 3221 (1994).
[21] Y. Zhou, A phenomenological treatment of rotating turbulence, Phys. Fluids **7**, 2092 (1995).
[22] J. Callies and R. Ferrari, Interpreting energy and tracer spectra of upper-ocean turbulence in the submesoscale range (1–200 km), J. Phys. Oceanogr. **43**, 2456 (2013).
[23] O. Bühler, J. Callies, and R. Ferrari, Wave–vortex decomposition of one-dimensional ship-track data, J. Fluid Mech. **756**, 1007 (2014).
[24] J. Callies, O. Bühler, and R. Ferrari, The dynamics of mesoscale winds in the upper troposphere and lower stratosphere, J. Atmos. Sci. **73**, 4853 (2016).
[25] H. A. Kafiabad, M. A. C. Savva, and J. Vanneste, Diffusion of inertia-gravity waves by geostrophic turbulence, J. Fluid Mech. **869**, R7 (2019).
[26] M. A. C. Savva, H. A. Kafiabad, and J. Vanneste, Inertia-gravity-wave scattering by three-dimensional geostrophic turbulence, J. Fluid Mech. **916**, A6 (2021).
[27] S. Nazarenko, *Wave Turbulence* (Springer Science & Business Media, Berlin Heidelberg, 2011), Vol. 825.
[28] S. Galtier, Weak inertial-wave turbulence theory, Phys. Rev. E **68**, 015301(R) (2003).
[29] S. G. Huisman, D. P. M. van Gils, S. Grossmann, C. Sun, and D. Lohse, Ultimate turbulent Taylor-Couette flow, Phys. Rev. Lett. **108**, 024501 (2012).
[30] X. Zhu, R. J. A. M. Stevens, O. Shishkina, R. Verzicco, and D. Lohse, $Nu \sim Ra^{1/2}$ scaling enabled by multiscale wall roughness in Rayleigh–Bénard turbulence, J. Fluid Mech. **869**, R4 (2019).
[31] H. Jiang, D. Wang, S. Liu, and C. Sun, Experimental evidence for the existence of the ultimate regime in rapidly rotating turbulent thermal convection, Phys. Rev. Lett. **129**, 204502 (2022).
[32] H. Brauckmann, B. Eckhardt, and J. Schumacher, Heat transport in rayleigh-bénard convection and angular momentum transport in taylor-couette flow: A comparative study, Philos. Trans. R. Soc. A **375**, 20160079 (2017).
[33] S. Zhang and C. Sun, Twin forces: similarity between rotation and stratification effects on wall turbulence, J. Fluid Mech. **979**, A45 (2024).

[34] J.-H. Xie and O. Bühler, Two-dimensional isotropic inertia-gravity wave turbulence, J. Fluid Mech. **872**, 752 (2019).

[35] W. R. Young and M. Ben Jelloul, Propagation of near-inertial oscillations through a geostrophic flow, J. Mar. Res. **55**, 735 (1997).

[36] A. J. Majda, D. W. McLaughlin, and E. G. Tabak, A one-dimensional model for dispersive wave turbulence, J. Nonlin. Sci. **7**, 9 (1997).

[37] A. N. Kolmogorov, Dissipation of energy in the locally isotropic turbulence, *Dokl. Akad. Nauk SSSR A* **32**, 16 (1941).

[38] K. S. Smith, G. Boccaletti, C. C. Henning, I. Marinov, C. Y. Tam, I. M. Held, and G. K. Vallis, Turbulent diffusion in the geostrophic inverse cascade, J. Fluid Mech. **469**, 13 (2002).

[39] P. Winchester, V. Dallas, and P. D. Howell, Two-dimensional rayleigh–bénard convection without boundaries, J. Fluid Mech. **998**, A27 (2024).

[40] G. K. Vallis and M. E. Maltrud, Generation of mean flows and jets on a beta plane and over topography, J. Phys. Oceanogr. **23**, 1346 (1993).

[41] E. A. Kochurin and E. A. Kuznetsov, Direct numerical simulation of acoustic turbulence: Zakharov–Sagdeev spectrum, JETP Lett. **116**, 863 (2022).